

# Journal of Materials Chemistry B

Accepted Manuscript



This is an *Accepted Manuscript*, which has been through the Royal Society of Chemistry peer review process and has been accepted for publication.

*Accepted Manuscripts* are published online shortly after acceptance, before technical editing, formatting and proof reading. Using this free service, authors can make their results available to the community, in citable form, before we publish the edited article. We will replace this *Accepted Manuscript* with the edited and formatted *Advance Article* as soon as it is available.

You can find more information about *Accepted Manuscripts* in the [Information for Authors](#).

Please note that technical editing may introduce minor changes to the text and/or graphics, which may alter content. The journal's standard [Terms & Conditions](#) and the [Ethical guidelines](#) still apply. In no event shall the Royal Society of Chemistry be held responsible for any errors or omissions in this *Accepted Manuscript* or any consequences arising from the use of any information it contains.

Cite this: DOI: 10.1039/c0xx00000x

www.rsc.org/xxxxxx

ARTICLE TYPE

# Nanoporous PdCr alloy as nonenzymatic electrochemical sensor for hydrogen peroxide and glucose

Dianyun Zhao,<sup>a</sup> Zhihong Wang,<sup>b</sup> Jinping Wang,<sup>a</sup> and Caixia Xu<sup>a\*</sup>

Received (in XXX, XXX) Xth XXXXXXXXX 20XX, Accepted Xth XXXXXXXXX 20XX

DOI: 10.1039/b000000x

Nanoporous (NP) PdCr alloy is easily fabricated through one step mild dealloying PdCrAl source alloy in NaOH solution. Electron microscopy demonstrates that dealloying PdCrAl alloy generates a bicontinuous spongy morphology with a narrow ligament size at ~5 nm. The as-made NP-PdCr alloy exhibits high sensing performance toward H<sub>2</sub>O<sub>2</sub>, such as a wide linear range from 0.1 to 1.9 mM, fast amperometric response, and a low detection limit of 3.1 μM. In particular, NP-PdCr alloy has distinct sensing durability with almost no activity loss upon continuous H<sub>2</sub>O<sub>2</sub> detection for two weeks. In addition, this nanostructure exhibits high activity for glucose sensing in a wide linear range from 1 to 38 mM, long-term stability, and it is also highly resistant toward poisoning by Cl<sup>-</sup>. Moreover, NP-PdCr shows a good anti-interference toward ascorbic acid, uric acid, and dopamine after coating additional nafion solution.

## 1. Introduction

Hydrogen peroxide (H<sub>2</sub>O<sub>2</sub>) is an essential mediator and an oxidizing agent involved in many chemical and biological processes.<sup>1,2</sup> Glucose is an important species in diabetes management and food industry.<sup>3-5</sup> Therefore, sensitive detection of H<sub>2</sub>O<sub>2</sub> and glucose is of great importance in environmental, pharmaceutical, and biomedical research in recent years.<sup>6,7</sup> Different analytical methods for the detection of H<sub>2</sub>O<sub>2</sub> and glucose have been reported, such as fluoroimmunoassay, colorimetric assay, artificial enzyme mimics, electrochemiluminescence etc.<sup>8-13</sup> Among these methods, electrochemical sensors based on electrocatalysis of small molecules over advanced nanomaterials have received considerable attention with the advantages of high sensitivity, easy operation, and fast detection to target molecules.<sup>14,15</sup>

Palladium nanomaterials exhibit great potentials for constructing highly effective electrochemical sensing platforms due to their unique electrocatalytic activity.<sup>16,17</sup> However, the surfaces of metals are easily poisoned by the adsorbed intermediates and chloride, leading to decreased sensitivity. It is reported that alloy nanomaterials, which combine the advantages of two compositions, have received considerable attention for synergistic catalytic effect between the two compositions.<sup>18</sup> Consequently, it is interesting to construct highly sensitive and stable electrochemical biosensors by using Pd-based alloy materials. Among various Pd-based alloy electrocatalysts, some metals have been found to be the favorable assistant elements for Pd to achieve better sensing performance as well enhance the utilization.<sup>19-22</sup> For instance, Behmenyar et al. prepared Pd/Cu supported catalysts by reducing palladium acetate and copper acetate in ethylene glycol solution, finding good electrocatalytic activity for sodium borohydride in direct borohydride fuel cell.<sup>23</sup>

Wang et al. synthesized Pd/Co nanoparticles by utilizing the distinction of reduction potential between Na<sub>2</sub>PdCl<sub>4</sub> and Co(NO<sub>3</sub>)<sub>2</sub>, finding durable stability for the hydrolytic dehydrogenation of ammonia borane.<sup>24</sup> Being indeed quite successful in achieving high activity, however, the preparation of these nanostructures is complicated involving a multi-step operation. In addition, their preparation process usually involves the usage of excessive organic agents or high temperature processing with low production yielding or with applied potential used to reduce the metal salts. Consequently, it is necessary to develop environmentally benign and effective fabrication route with desired properties to construct highly effective electrochemical sensors.

At present, nanoporous (NP) Pd-based structures have attracted great attention due to their interconnected nanoscaled skeleton and porous channels, which are preferable for unblocked mass and electron transport.<sup>25-27</sup> Nanoporous Pd-based alloy prepared by dealloying have some advantages in easy operation, no particle aggregation, extremely clean metal surface, and superior stability.<sup>28</sup> In current work, NP-PdCr alloy was fabricated by selectively dealloying the ternary PdCrAl source alloy in NaOH solution. As a 3d metal, Cr is widely used because of its stability and has exhibited synergistic catalytic effect on electrocatalytic reactions of Pd such as formic acid electrooxidation.<sup>29</sup> The sensing performances of the NP-PdCr alloy were studied toward H<sub>2</sub>O<sub>2</sub> and glucose as models. The experimental results demonstrated that NP-PdCr is preferable for constructing highly sensitive and stable electrochemical sensors.

## 2. Experimental

Pd<sub>15</sub>Cr<sub>5</sub>Al<sub>80</sub> and Pd<sub>20</sub>Al<sub>80</sub> alloy foils were made by refining pure Pd, Cr, and Al (99.99 %) in an arc-furnace, respectively, followed by melt-spinning under Ar-protected atmosphere. NP-PdCr and

NP-Pd were prepared by etching PdCrAl and PdAl alloy foils in 0.5 M NaOH for 48 hours at room temperature, respectively.  $\text{H}_2\text{O}_2$  (30 %) and glucose were purchased from Sinopharm Chemical Reagent Co. Ltd. The phosphate buffered saline (0.1 M PBS, pH 7.0) solution was prepared using  $\text{Na}_2\text{HPO}_4$  and  $\text{KH}_2\text{PO}_4$ . Ultra-pure water (18.2 M $\Omega$ ) was used in all measurements. Ascorbic acid (AA), uric acid (UA), and dopamine (DA) were purchased from Sigma-Aldrich. All the reagents were of analytical reagents grade and used without further treatment.

Powder X-ray diffraction (XRD) was carried out on a Bruker D8 advanced X-ray diffractometer using Cu KR radiation at a step rate of  $0.04^\circ \text{s}^{-1}$ . The structure characterizations were carried out on a JEM-2100 transmission electron microscope (TEM) and a JSM-6700 field-emission scanning electron microscope (SEM) equipped with an Oxford INCA x-sight Energy Dispersive X-ray Spectrometer (EDS). All electrochemical measurements were performed using CHI 760D electrochemical workstation (Shanghai CH Instruments Co., China). A conventional three-electrode cell was used with Pt foil as a counter electrode, mercury sulfate electrode as the reference electrode, and 4-mm-diameter glassy carbon electrode as work electrode.

Catalyst ink was prepared by mixing 1.5 mg carbon powder, 1.0 mg NP-PdCr, 400  $\mu\text{L}$  isopropanol, and 200  $\mu\text{L}$  nafion solutions (0.5 wt. %) under sonication for 30 min. The working electrode was made by dropping appropriate catalyst ink on a polished glassy carbon electrode and dried. The NP-Pd and Pd/C electrodes were prepared in a similar way. The electrochemical surface areas (ECSA) of Pd in all catalysts were evaluated by integrating the reduction charges during the stripping of surface monolayer oxide in  $\text{N}_2$ -purged 0.5 M  $\text{H}_2\text{SO}_4$  solution in the range of 0 to 1.35 V at the scan rate of  $50 \text{ mV} \cdot \text{s}^{-1}$ , in which the used charge density is  $420 \mu\text{C} \cdot \text{cm}^{-2} \text{Pd}$ .

### 3. Results and discussion

#### 3.1 Characterization of NP-PdCr alloy

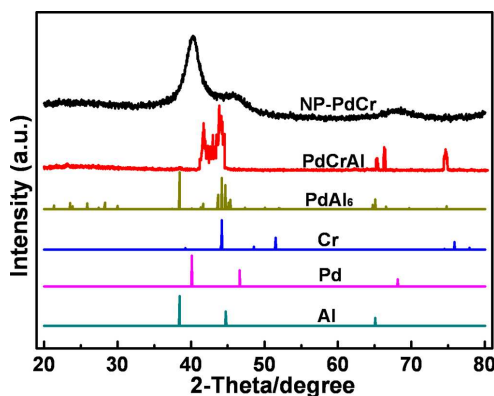


**Fig. 1.** XRD patterns of  $\text{Pd}_{15}\text{Cr}_5\text{Al}_{80}$  and the dealloyed sample, the standard patterns of Pd (JCPDS 65-2867), Cr (JCPDS 65-3316),  $\text{PdAl}_6$  (JCPDS 42-1286), and Al (JCPDS 65-2869) are also attached for clear comparison.

To gain insight into the structural formation and evolution, XRD was employed to examine the crystal structures of the precursor and obtained sample. As shown in Fig. 1, the  $\text{PdCrAl}$  precursor exhibited a series of diffraction peaks, which can be assigned to a

$\text{PdAl}_6$ -type crystal structure. EDS (Fig. S1a) analysis shows the composition of the precursor is  $\text{Pd}_{15}\text{Cr}_5\text{Al}_{80}$  (at.%), which is consistent with the initial feeding ratio during alloy refining. It is noted that the relative intensity and peak position of these diffraction peaks are different from the standard  $\text{PdAl}_6$  diffraction pattern, which may be caused by the different alloy composition and the rapid solidification processing during alloy refining. The dealloyed PdCr sample showed only a set of broad diffraction peaks with  $2\theta$  values at around 40.5, 46.2, 68.3. These peaks can be assigned to the (111), (200), (220) diffractions for a face centered cubic PdCr alloy. It is also noted that there are no additional diffraction peaks emerged related to individual Pd and Cr (or its oxides), indicating the formation of a homogenous single-phase PdCr alloy. The leaching of Al resulted in obvious evolution of the diffraction peaks similar to those of pure Pd. Moreover, the difference between NP-PdCr and pure Pd in peak positions is still visible, which implies the persistence of alloyed Cr to Pd. The broad diffraction features in the PdCr sample mainly arise from the large surface strain formed during dealloying because of the smaller ligament size and smaller grain size. EDS (Fig. S1b) data indicates that a majority of Al atoms were removed with little Al atoms remained in the resulted sample. Moreover, the bimetallic composition between Pd and Cr in the resulted sample basically maintained the initial feeding ratio, suggesting the better control for the alloy components.

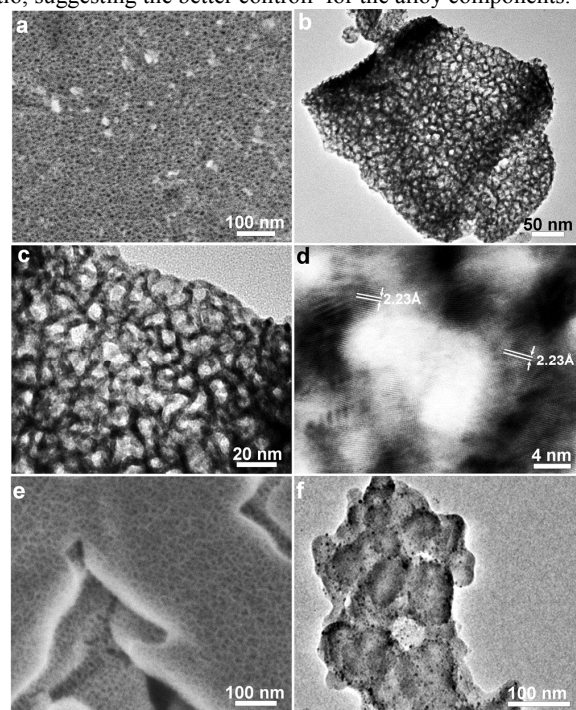


**Fig. 2.** SEM (a), TEM (b, c) and HRTEM (d) images of the resulted samples by dealloying  $\text{Pd}_{15}\text{Cr}_5\text{Al}_{80}$  alloy in 0.5 M NaOH solution for 48 h at room temperature, (e) SEM image of NP-Pd, (f) TEM image of Pd/C.

Fig. 2 (a-d) shows the resulted nanostructure by dealloying of  $\text{PdCrAl}$  alloy in 0.5 M NaOH solution for 48 h at room temperature. From the surface SEM image in Fig. 2a, it can be clearly observed that selectively etching Al successfully generated a bicontinuous spongy morphology with a narrow

ligament size at  $\sim 5$  nm. The dark ligaments and bright pores in the TEM image (Fig. 2b, c) of the sample further indicate the formation of nanoporous structure. Fig. 2d provides a high-resolution TEM (HRTEM) image of the sample, in which the continuous ordered lattice fringes are well resolved. Fig. 2e gives the SEM image of NP-Pd, which also shows bicontinuous nanoporous structure with uniform ligament distribution. The TEM image of Pd/C was shown in Fig. 2f, from which it is clear that Pd nanoparticles disperse on the carbon support with the particle size around 3-5 nm.

### 3.2. Electrocatalytic measurements of $\text{H}_2\text{O}_2$ on NP-PdCr

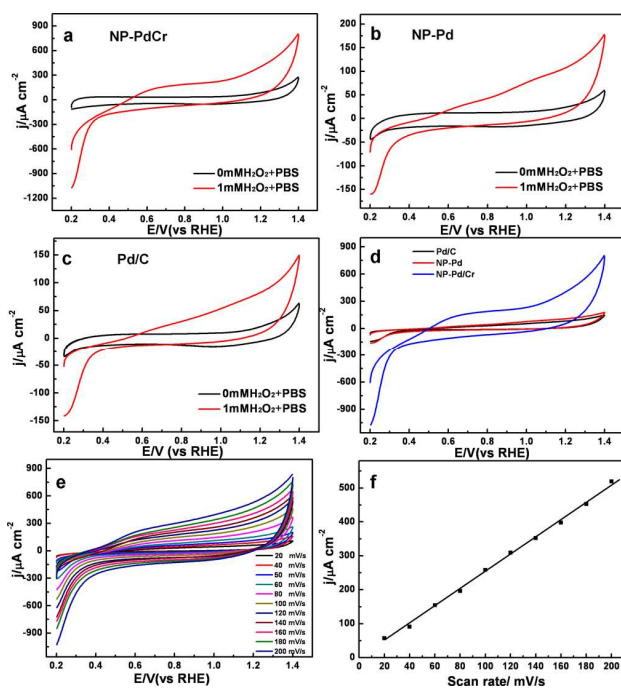


**Fig. 3.** CV curves of (a) NP-PdCr, (b) NP-Pd, (c) Pd/C in PBS solution with and without 1 mM  $\text{H}_2\text{O}_2$ . (d) CV curves of all samples in PBS + 1 mM  $\text{H}_2\text{O}_2$  solution. (e) CV curves of NP-PdCr in PBS + 1 mM  $\text{H}_2\text{O}_2$  solution at different scan rates of 20, 40, 60, 80, 100, 120, 140, 160, 180, and 200 mV/s. (f) Plots of current on NP-PdCr at 1.2 V.

Characterized by the desirable nanoporous architecture with bicontinuous skeleton and hollow interconnected channels, NP-PdCr is favorable for the molecules transport and electron conductivity.<sup>30</sup> Consequently, it is interesting to explore the sensing performance of NP-PdCr alloy toward  $\text{H}_2\text{O}_2$ . Fig. 3 shows the cyclic voltammetric (CV) curves of Pd/C, NP-Pd, and NP-PdCr modified electrode in PBS solution in the presence and absence of  $\text{H}_2\text{O}_2$ . It is observed that NP-PdCr alloy exhibits higher oxidation current toward  $\text{H}_2\text{O}_2$  starting from 0.5 V compared with that in pure PBS solution (Fig. 3a). The current density for  $\text{H}_2\text{O}_2$  oxidation on NP-PdCr in the range of 0.9-1.2 V is more than 4 times higher than those of Pd/C and NP-Pd catalysts, while the onset oxidation potential negatively shifted more than 50 mV (Fig. 3a-d). It is clear that NP-PdCr shows much higher electrocatalytic activity toward  $\text{H}_2\text{O}_2$  oxidation compared with NP-Pd and Pd/C catalysts. The electrocatalytic behaviour of NP-PdCr toward  $\text{H}_2\text{O}_2$  oxidation was further

investigated by changing the scan rate. As displayed in Fig. 3e, the currents at 1.2 V are linear as a function of the scan rate in a range from 20 to 200 mV/s and the corresponding linear equation for the currents is  $I (\mu\text{A}) = -1.92 + 2.55 v$  with a linear correlation coefficient of 0.997. This indicates that the electrochemical oxidation of  $\text{H}_2\text{O}_2$  on the NP-PdCr modified electrode is a surface-controlled process.<sup>31</sup> It can be concluded that as-prepared NP-PdCr alloy has greatly enhanced catalytic activities toward  $\text{H}_2\text{O}_2$ , providing a substantial basis for its electrochemical sensing application.

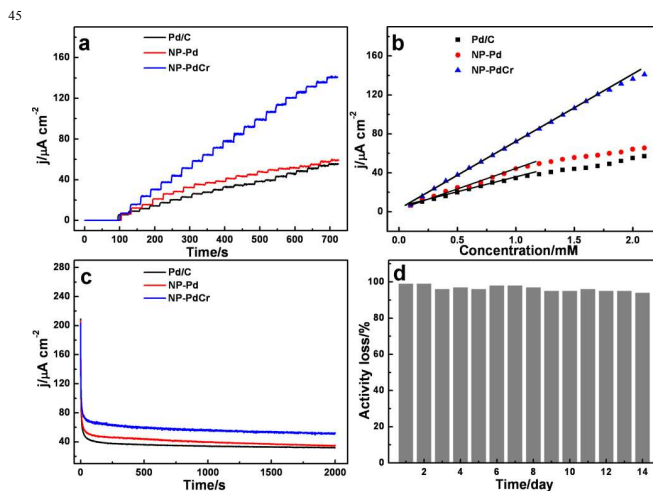


**Fig. 4.** (a) Amperometric responses of NP-Pd, Pd/C, and NP-PdCr alloy on successive addition of 0.1 mM  $\text{H}_2\text{O}_2$  into stirring PBS solution at 1.2 V. (b) Plots of current vs.  $\text{H}_2\text{O}_2$  concentrations. (c) Sensing stability of NP-Pd, Pd/C, and NP-PdCr alloy in a stirred PBS solution containing 1 mM  $\text{H}_2\text{O}_2$  for 2000s at 1.2 V. (d) Long-term stability of NP-PdCr alloy for continuous  $\text{H}_2\text{O}_2$  detection for 14 days.

Based on the high oxidation activity toward  $\text{H}_2\text{O}_2$ , the sensing performance of NP-PdCr alloy is evaluated by amperometric detection upon the successive addition of  $\text{H}_2\text{O}_2$ . Fig. 4a shows the typical amperometric responses of Pd/C, NP-Pd, and NP-PdCr alloy at a fixed potential. Noting that NP-PdCr electrode responds rapidly ( $\sim 1.5$  s) to each addition of  $\text{H}_2\text{O}_2$ . The rapid response could be attributed to the fact that  $\text{H}_2\text{O}_2$  could diffuse freely into the bicontinuous nanoporous structure as well rapidly be oxidized on the NP-PdCr surface. In comparison, NP-PdCr electrode shows higher response signals to the each addition of  $\text{H}_2\text{O}_2$  compared with NP-Pd and Pd/C electrodes. As shown in Fig. 4b, NP-Pd catalyst has a linear response to  $\text{H}_2\text{O}_2$  in the range of 0.1 to 1.0 mM (linear equation:  $y = 42.51 x + 3.68$ ,  $R = 0.991$ ) with a detection limit of  $\sim 4.5 \mu\text{M}$  ( $S/N=3$ ). And the Pd/C sample performs better linear relationship in the range of 0.1 to 1.0 mM (linear equation:  $y = 29.41 x + 4.72$ ,  $R = 0.993$ ) with a detection limit of  $\sim 3.8 \mu\text{M}$ . By comparison, NP-PdCr alloy exhibits the highest sensitivity and the widest linear range up to 1.9 mM (linear equation:  $y = 68.76 x + 2.84$ ,  $R = 0.998$ ) with the lowest detection limit of  $\sim 3.1 \mu\text{M}$ . These analytical parameters of NP-PdCr are better than other reported catalysts based  $\text{H}_2\text{O}_2$  sensors as shown in Table 1.<sup>1, 32-35</sup> The remarkable performance of NP-PdCr modified electrode toward the detection of  $\text{H}_2\text{O}_2$  indicates that NP-PdCr holds great potential to construct  $\text{H}_2\text{O}_2$  sensor.

**Table 1** A comparison of the performance of some sensor platforms using different electrodes for H<sub>2</sub>O<sub>2</sub> detection.

H <sub>2</sub> O <sub>2</sub> sensor	Linear Range (mM)	Sensitivity ( $\mu\text{Acm}^{-2}\text{mM}^{-1}$ )	Detection limit ( $\mu\text{M}$ )	Ref.
Cu NCs	0.01-1.00	---	10	32
Graphene-AuNPs/GCE	0.02-0.28	3000	6	33
Nafion/HRP/TN-3/ITO	0.001-0.78	1176	0.18	1
Palladized aluminum	0.005-0.034	---	4.0	34
PtPd/MWCNs/GC	0.0025-0.125	414.8	1.2	35
NP-PdCr	0.1-1.9	72	3.1	This work

The long-term catalytic activity of the NP-PdCr alloy was evaluated by studying its steady-state activity using potentiostatic method. As is shown in Fig. 4c, NP-PdCr shows a more stable amperometric response to the addition of 1 mM H<sub>2</sub>O<sub>2</sub> in stirring PBS after running for 2000 s compared with NP-Pd and Pd/C, indicating the higher sensing durability. The reproducibility of NP-PdCr electrodes was further explored by continuous detecting H<sub>2</sub>O<sub>2</sub> every day for a period of two weeks. As shown in Fig. 4d, the current response of the electrode has little change over a period of 14-day. Only 6.9 % degradation in current was detected within two weeks, demonstrating that NP-PdCr is highly stable and repeatable to H<sub>2</sub>O<sub>2</sub> detection. The relative standard deviation (RSD) for 0.5 mM H<sub>2</sub>O<sub>2</sub> on NP-PdCr is calculated to be ~1.7 %. For three NP-PdCr modified electrodes, the RSD is 3.2 %. It is demonstrated that NP-PdCr shows good long-term stability and reproducibility for H<sub>2</sub>O<sub>2</sub> detection.

### 3.3. Electrocatalytic measurements of glucose on NP-PdCr

Fig. 5a presents the CV response of NP-PdCr modified electrode in 0.1 M NaOH solution with and without glucose. It is observed that the NP-PdCr electrode exhibits high oxidation currents starting from -0.3 V in the presence of glucose. The anodic peak located at 0.2 V could be attributed to glucose electroadsorption, causing the generation of adsorbed intermediates.<sup>36</sup> However, the accumulation of the intermediates on the electrode surface inhibited the further electroadsorption of glucose, resulting in current decrease. When the potential was larger than 0.6V, Pd-OH species are generated in the alkaline solution. Pd-OH species are beneficial in oxidation of intermediates on PdCr surface, causing the current increase again. Moreover, the electrooxidation current also increased due to the direct oxidation of glucose on the surface. In the negative scan, the oxidized Pd are reduced at a potential around 0.1 V. With the backward scan, more surface-active sites were refreshed and became available for the oxidation of glucose, resulting in a large anodic peak in the potential around -0.1 V. Meanwhile, the accumulation of intermediates again occurred, inducing the current decrease. It is obvious that the NP-PdCr shows similar electrochemical behavior to NP-Pd and Pd/C for glucose oxidation. However, compared with NP-Pd and Pd/C catalysts, the much higher current density on NP-PdCr indicates greatly enhanced catalytic activities toward glucose

45 electrooxidation due to the synergetic catalytic effect of Pd and Cr.

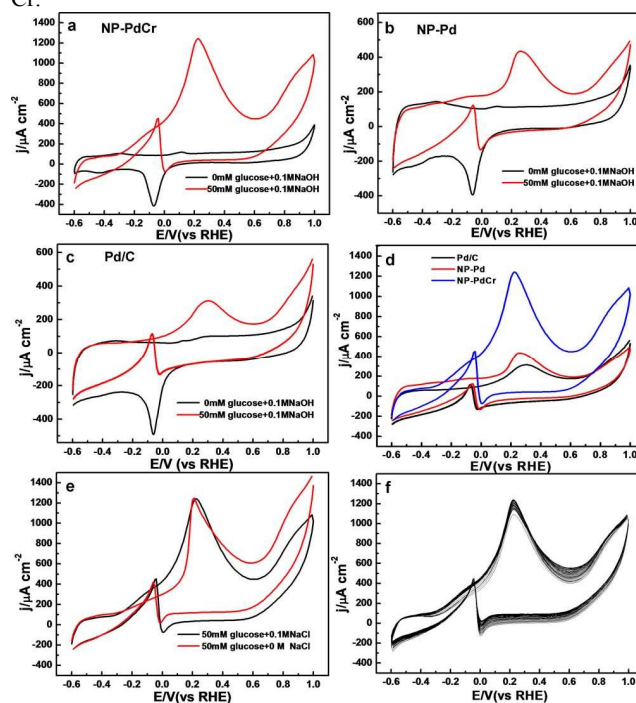


**Fig. 5.** CV curves of (a) NP-PdCr, (b) NP-Pd, and (c) Pd/C in 0.1 M NaOH solution with the presence and absence of 50 mM glucose. (d) CV curves of NP-Pd, Pd/C, and NP-PdCr in 50 mM glucose and 0.1 M NaOH solution. (e) CV curves of NP-PdCr alloy in 0.1 M NaOH and 50 mM glucose solution with and without 0.1 M NaCl. (f) CV curves (50 cycles) of NP-PdCr alloy in 0.1 M NaOH and 50 mM glucose solution.

It has been reported that Cl<sup>-</sup> has a serious poisoning effect on some metallic electrocatalysts, leading to the activity loss toward the glucose electrooxidation.<sup>36</sup> Fig. 5e shows the CV curves of NP-PdCr alloy in 0.1 M NaOH and 50 mM glucose solution with and without NaCl. The glucose oxidation activity on NP-PdCr has almost no change after adding NaCl, suggesting that NP-PdCr can well maintain its catalytic property in the presence of Cl<sup>-</sup>. However, it is noted that the current at 0.9 V became higher after adding Cl<sup>-</sup>, which is consistent with the previous reports in Cl<sup>-</sup> poisoning effect on some catalysts.<sup>37</sup> Fig. 5f shows the CV evolution of NP-PdCr during continuous potential scan. It is found that the current almost unchanged after 50 cycles, indicating the good electrocatalytic durability of NP-PdCr catalyst.

The long-term sensing stability of NP-PdCr electrocatalysts is significant for continuous and reliable monitoring of glucose. The long-term sensing ability of NP-PdCr alloy for glucose sensing was evaluated by detecting the steady-state specific activity using potentiostatic method. As is shown in Fig. 6a, NP-PdCr shows a higher sensing durability and more stable amperometric response to the addition of 10 mM glucose in stirring NaOH after running for 2000 s compared with NP-Pd and Pd/C. Fig. 6b shows the typical amperometric response of NP-PdCr alloy toward the successive addition of glucose at a fixed potential. NP-PdCr electrode responds rapidly to each addition of glucose and reaches the maximum steady-state current within 1.8 s. The rapid response could be attributed to the fact that glucose could diffuse

freely into the bicontinuous nanoporous structure as well rapidly be oxidized on NP-PdCr surface. In comparison, NP-PdCr electrode shows higher current response signals to the addition of glucose compared with NP-Pd and Pd/C electrodes with the current response intensity in NaOH system due to the synergistic effect between Cr and Pd atoms. As shown in Fig. 6c, the NP-PdCr alloy exhibits the high sensitivity and wide linear range up to 38 mM (linear equation:  $y = 1.57 + 0.43x$ ,  $R = 0.996$ ) with the lowest detection limit of 1.8  $\mu\text{M}$ . In comparison, the sensing range of Pd/C and NP-Pd are respective up to 16 mM and 14 mM (linear equation:  $y = 0.57 + 0.23x$ ,  $R = 0.986$  and  $y = 0.46 + 0.36x$ ,  $R = 0.996$ ) with the detection limit of 2.1  $\mu\text{M}$  and 2.3  $\mu\text{M}$ . The analytical parameters of NP-PdCr are better than other reported catalysts based glucose sensors as shown in Table 2.<sup>17, 22, 36, 38, 39</sup>

The better performance of NP-PdCr modified electrode toward the detection of glucose indicates that NP-PdCr holds great potential to construct glucose sensor.

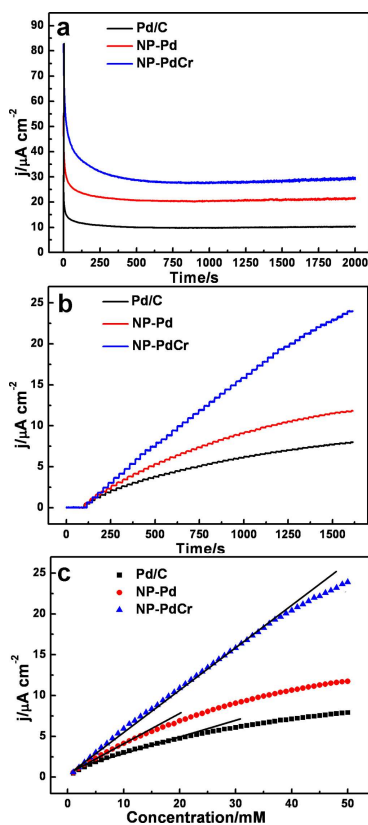


**Fig. 6.** (a) Sensing stability NP-Pd, Pd/C, and NP-PdCr alloy in a stirred NaOH solution containing 10 mM glucose for 2000 s at 0.35 V. (b) Amperometric current responses of NP-Pd, Pd/C and NP-PdCr on successive addition of 1 mM glucose into stirring NaOH solution at 0.35 V. (c) Plots of current vs. glucose concentrations.

25

**Table 2** A comparison of the performance of some sensor platforms using different electrodes for glucose detection.

Glucose sensor	Linear range (mM)	Sensitivity ( $\mu\text{Acm}^{-2} \text{mM}^{-1}$ )	Applied potential	Ref.
Cu film	0.001-0.5	699.45	+0.40	38
GoX/Pt/OMC	0.050-3.7	0.38	+0.60	39
GOx/Pd NPs	0.040-22	---	+0.25	17
Pd-Ni/SiNWs	0-20	190.72	+0.14	40
PdNPs-FCNTs-Nafion	0-46	11.4	+0.40	36
NP-PdCr	1-38	0.75	+0.35	This work

### 3.4 The anti-interference for electrochemical detection of $\text{H}_2\text{O}_2$ and glucose on NP-PdCr

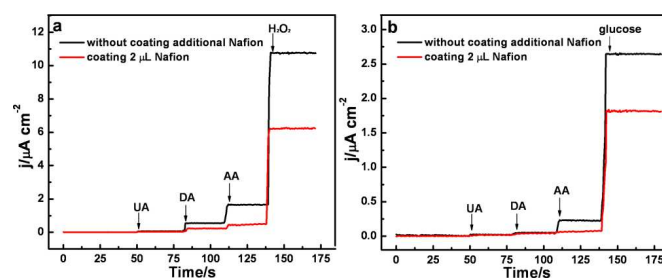


**Fig. 7.** Interference (0.02 mM UA, 0.01 mM DA, and 0.1 mM AA) on the response of (a) 1 mM  $\text{H}_2\text{O}_2$  in 0.1 M PBS solution at 1.2 V and (b) 10 mM glucose in 0.1 M NaOH solution at 0.35 V.

One of the major challenges in nonenzymatic  $\text{H}_2\text{O}_2$  and glucose detections is the interfering electrochemical signals caused by some easily oxidizable compounds such as AA, UA, and DA. So, it is essential to investigate the anti-interference of NP-PdCr toward the  $\text{H}_2\text{O}_2$  and glucose sensing. Fig. 7a shows the chronoamperometry curves of NP-PdCr electrode with successive addition of 0.02 mM UA, 0.01 mM DA, 0.1 mM AA, and 1 mM  $\text{H}_2\text{O}_2$ . The interferences from UA, DA or AA were 0.4 %, 4.7 % or 9.1 % of the response generated by  $\text{H}_2\text{O}_2$  on NP-PdCr modified electrode. It has found that nafion solution coated on the electrodes can form a thin film to exclude the interference of these electroactive molecules.<sup>40</sup> After coating extra 2  $\mu\text{L}$  nafion, interferences became 0.1 %, 3.7 % or 3.2 %. In addition, Fig. 7b shows the influence of DA, UA, and AA toward glucose detection. The interferences from UA, DA or AA were 0.8 %, 1.1 % or 6.5 % of the response generated by glucose on NP-PdCr modified electrode. After coating extra 2  $\mu\text{L}$  nafion, they became 0.8 %, 1.1 % or 3.8 % respectively. The result demonstrated that electrochemical detection of  $\text{H}_2\text{O}_2$  and glucose on NP-PdCr-Nafion modified electrodes could be performed with little interference from DA, UA, and AA by coating the extra nafion solution.

## 4. Conclusions

In this work, NP-PdCr alloy is successfully fabricated with bicontinuous nanoporous architecture by a simple dealloying strategy. It is clear that NP-PdCr shows much higher

electrooxidation activities toward H<sub>2</sub>O<sub>2</sub> and glucose compared with NP-Pd and Pd/C catalysts. Compared with NP-Pd, alloying Pd with Cr greatly enhanced the catalytic activities toward H<sub>2</sub>O<sub>2</sub> and glucose electrooxidation due to the alloying effect. Compared with Pd/C catalyst, the higher electrocatalytic activity of NP-PdCr alloy may be due to the the unique nanoporous structures besides the alloying effect. In the nanoporous structure the bicontinuous void space provides the integral molecular transport paths, and the interconnected nanoscaled skeleton makes the easy transport of electrons and adsorbed reaction medium, which is preferable for the electrocatalysis reactions. Based on the unique electrocatalytic activities, NP-PdCr can achieve sensitive detection for H<sub>2</sub>O<sub>2</sub> and glucose with wide concentration range and fast response. NP-PdCr also shows a long-term sensing durability and reproducibility toward H<sub>2</sub>O<sub>2</sub> and glucose with the structural advantage as well little interference from DA, UA, and AA. Along with these attractive features, NP-PdCr alloy holds great potential in electrochemical sensors.

### Acknowledgements

This work was supported by the National Science Foundation of China (51001053, 21271085).

### Notes and references

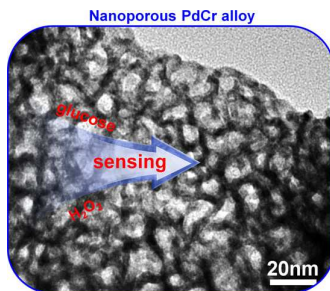
<sup>a</sup>Key Laboratory of Chemical Sensing & Analysis in Universities of Shandong, School of Chemistry and Chemical Engineering, University of Jinan, Jinan, 250022, China.

Fax: +86-531-82765969; Tel: +86-531-89736103; E-mail: chm\_xucx@ujn.edu.cn

<sup>b</sup>School of Basic Medical Sciences, Shandong University of Traditional Chinese Medicine, Jinan 250355

### References

- Q. Li, K. Cheng, W. J. Weng, P. Y. Du and G. R. Han, *J. Mater. Chem.*, 2012, **22**, 9019-9026.
- J. D. Gaynor, A. S. Karakoti, T. Inerbaev, S. Sanghavi, P. Nachimuthu, V. Shutthanandan, S. Seal and S. Thevuthasan, *J. Mater. Chem. B*, 2013, **1**, 3443-3450.
- A. Ciszewski and I. Stepniak, *Electrochim. Acta* 2013, **111**, 185-191.
- K. J. Chen, W. N. Su, C. J. Pan, S. Y. Cheng, J. Rick, S. H. Wang, C. C. Liu, C. C. Chang, Y. W. Yang, C. H. Wang and B. J. Hwang, *J. Mater. Chem. B*, 2013, **1**, 5925-5932.
- M. Ammann and J. Fransaer, *Biosens. Bioelectron.*, 2013, **39**, 274-281.
- C. X. Xu, J. Q. Wang and J. H. Zhou, *Sens. Actuators. B* 2013, **182**, 408-415.
- A. Walcarius, S. D. Minter, J. Wang, Y. H. Lin and A. Merkoçi, *J. Mater. Chem. B*, 2013, **1**, 4878-4908.
- T. Wen, F. Qu, N. B. Li and H. Q. Luo, *Anal. Chim. Acta.*, 2012, **749**, 56-62.
- J. J. Wang, D. X. Han, X. H. Wang, B. Qi and M. S. Zhao, *Biosens. Bioelectron.*, 2012, **36**, 18-21.
- Y. F. Cheng, R. Yuan, Y. Q. Chai, H. Niu, Y. L. Cao, H. J. Liu, L. J. Bai and Y. L. Yuan, *Anal. Chim. Acta.*, 2012, **745**, 137-142.
- M. Abo, Y. Urano, K. Hanaoka, T. Terai, T. Komatsu and T. Nagano, *J. Am. Chem. Soc.*, 2011, **133**, 10629-10637.
- N. Anwar, M. Vagin, F. Laffir, G. Armstrong and T. McCormac, *Analyst* 2012, **137**, 624-630.
- L. P. Jia, J. F. Liu and H. S. Wang, *Electrochim. Acta.*, 2013, **111**, 411-418.
- Y. Xiang and Y. Lu, *Nat. Chem.*, 2011, **3**, 697-703.
- L. P. Jia and H. S. Wang, *Sens. Actuators. B* 2013, **177**, 1035-1042.
- G. Z. Hu, F. Nitze, T. Sharifi, H. R. Barzegar and T. Wågberg, *J. Mater. Chem.*, 2012, **22**, 8541-8548.
- M. Han, S. L. Liu, J. C. Bao and Z. H. Dai, *Biosens. Bioelectron.* 2012, **31**, 151-156.
- L. C. Jiang and W. D. Zhang, *Biosens. Bioelectron.* 2010, **25**, 1402-1407.
- Y. Q. Liu and C. X. Xu, *ChemSusChem* 2013, **6**, 78-84.
- C. Z. Zhu, S. J. Guo and S. J. Dong, *J. Mater. Chem.*, 2012, **22**, 14851-14855.
- Z. H. Zhang, C. Zhang, J. Z. Sun, T. Y. Kou, Q. G. Bai, Y. Wang and Y. Ding, *J. Mater. Chem. A*, 2013, **1**, 3620-3628.
- L. Y. Chen, H. Guo, T. Fujita, A. Hirata, W. Zhang, A. Inoue and M. W. Chen, *Adv. Funct. Mater.*, 2011, **21**, 4364-4370.
- G. Behmenyar and A. N. Akın, *J. Power Sources*, 2014, **249**, 239-246.
- J. Wang, Y. L. Qin, X. Liu and X. B. Zhang, *J. Mater. Chem.*, 2012, **22**, 12468-12470.
- P. J. Cappillino, J. D. Sugar, M. A. Hekmaty, B. W. Jacobs, V. Stavila, P. G. Kotula, J. M. Chames, N. Y. Yang and D. B. Robinson, *J. Mater. Chem.*, 2012, **22**, 14013-14022.
- C. X. Xu, Y. Q. Liu, H. Zhang and H. R. Geng, *Chem-Aian J.* 2013, **8**, 2721-2728.
- L. F. Liu and E. Pippel, *Angew. Chem. Int. Ed.* 2011, **50**, 2729-2733.
- C. X. Xu, Y. Q. Liu, Q. Hao and H. M. Duan, *J. Mater. Chem. A*, 2013, **1**, 13542-13548.
- W. J. Wen, C. Y. Li, W. P. Li and Y. Tian, *Electrochim. Acta.*, 2013, **109**, 201-206.
- C. X. Xu, F. L. Sun, H. Gao and J. P. Wang, *Anal. Chim. Acta.*, 2013, **780**, 20-27.
- J. P. Wang, D. F. Thomas and A. C. Chen, *Anal. Chem.*, 2008, **80**, 997-1004.
- L. Z. Hu, Y. L. Yuan, L. Zhang, J. M. Zhao, S. Majeed, G. B. Xu, *Anal. Chim. Acta*, 2013, **762**, 83-86.
- J. G. Hu, F. H. Li, K. K. Wang, D. X. Han, Q. X. Zhang, J. H. Yuan and L. Niu, *Talanta* 2012, **93**, 345-349.
- M. H. Pournaghi-Azar, F. Ahour and F. Pournaghi-Azar, *Sens. Actuators B*, 2010, **145**, 334-339.
- K. J. Chen, K. C. Pillai, J. Rick, C. J. Pan, S. H. Wang, C. C. Liu and B. J. Hwang, *Biosens. Bioelectron.*, 2012, **33**, 120-127.
- X. M. Chen, Z. J. Lin, D. J. Chen, T. T. Jia, Z. M. Cai, X. R. Wang and X. Chen, *Biosens. Bioelectron.*, 2010, **25**, 1803-1808.
- K. N. Heck, M. O. Nutt, P. Alvarez and M. S. Wong, *J. Catal.*, 2009, **267**, 97-104.
- F. Sun, L. Li, P. Liu and Y. F. Lian, *Electroanalysis* 2011, **23**, 395-401.
- X. Y. Jiang, Y. H. Wu, X. Y. Mao, X. J. Cui and L. D. Zhu, *Sens. Actuators B* 2011, **153**, 158-163.
- S. C. Hui, J. Zhang, X. J. Chen, H. H. Xu, D. F. Ma, Y. L. Liu and B. R. Tao, *Sens. Actuators, B*, 2011, **155**, 592-597.
- H. J. Qiu, L. Y. Xue, G. L. Ji, G. P. Zhou, X. R. Huang, Y. B. Qu and P. J. Gao, *Biosens. Bioelectron.*, 2009, **24**, 3014-3018.

**Graphical Abstract:**

Nanoporous PdCr alloy fabricated by one-step mild dealloying exhibits superior sensing performance and durability toward  $\text{H}_2\text{O}_2$  and glucose than Pt/C and NP-Pd catalysts.